

# Lepton-pair production in ultraperipheral collisions at AFTER@LHC

---

J.P. Lansberg<sup>a</sup> L. Szymanowski<sup>b</sup> J. Wagner<sup>b</sup>

<sup>a</sup>*IPNO, Université Paris-Sud, CNRS/IN2P3, F-91406, Orsay, France*

<sup>b</sup>*National Centre for Nuclear Research (NCBJ), Hoża 69, 00-681, Warsaw, Poland*

*E-mail:* [Jean-Philippe.Lansberg@in2p3.fr](mailto:Jean-Philippe.Lansberg@in2p3.fr), [Lech.Szymanowski@fuw.edu.pl](mailto:Lech.Szymanowski@fuw.edu.pl),  
[Jakub.Wagner@ncbj.gov.pl](mailto:Jakub.Wagner@ncbj.gov.pl)

**ABSTRACT:** We investigate the potentialities offered by the study of lepton-pair production in ultraperipheral collisions at a fixed-target experiment using the proton and ion LHC beams. In these collisions, exclusive or semi-exclusive lepton-pair production can be used as luminosity monitor as well as a check of the equivalent-photon approximation, via the measurement of the Bethe-Heitler cross section. It can also serve as a probe of the inner hadron structure via the measurement of the lepton-pair azimuthal asymmetry which is sensitive to the timelike virtual Compton scattering. We also briefly discuss the possibility offered by the study of  $\eta_c$  production. Finally, we outline the possibilities for lepton-pair production by Pomeron-Odderon fusion in exclusive  $pp$  and  $pA$  collisions.

---

## Contents

|          |  |           |
|----------|--|-----------|
| <b>1</b> | <b>Introduction.</b>   | <b>1</b>  |
| <b>2</b> | <b>Ultrapерipheral collisions in a high-energy fixed-target experiment</b>                           | <b>2</b>  |
| 2.1      | Generalities on photon-induced reactions in ultraperipheral collisions                               | 2         |
| 2.2      | Photon fluxes  | 4         |
| 2.3      | Fluxes and the rapidity dependence of the produced particles   | 6         |
| 2.3.1    | Single-photon case   | 6         |
| 2.3.2    | Double-photon case   | 9         |
| <b>3</b> | <b>Lepton-pair production: energy, invariant-mass, rapidity and transverse-momentum dependencies</b> | <b>9</b>  |
| 3.1      | Total cross section and for fixed $Q$  | 10        |
| 3.2      | Production at nonzero transverse momenta   | 12        |
| <b>4</b> | <b>Timelike compton scattering or exclusive photoproduction of a dilepton</b>                        | <b>13</b> |
| <b>5</b> | <b>Exclusive lepton-pair hadroproduction via odderon-pomeron fusion</b>                              | <b>17</b> |
| <b>6</b> | <b>Conclusion</b>  | <b>18</b> |
| <b>A</b> | <b>Kinematics</b>  | <b>20</b> |
| <b>B</b> | <b>Compton form factors and generalised parton distributions</b>                                     | <b>21</b> |

---

## 1 Introduction.

With the advent of RHIC and the LHC, the first experimental studies of Ultra-Peripheral Collisions (UPC) have successfully been carried out. The STAR collaboration first measured the  $\rho_0$  production cross section in AuAu UPC [1], then they measured the di-electron production cross section in UPC [2]. A little later the PHENIX collaboration released their first study of the  $J/\psi$  cross section as well as high-mass di-electron production [3]. More recently, further studies have been carried out at the LHC by the ALICE collaboration [4, 5].

Attempts to isolate UPC in InIn collisions in the fixed-target mode at the SPS have been made<sup>1</sup>. They were not conclusive, most probably because of the limited nucleon-nucleon centre-of-mass (cms) energy, on the order of 20 GeV, resulting in typical photon-nucleon cms energies below 3 GeV.

In this context, we investigate the possibility to study lepton-pair production in ultraperipheral collisions at a fixed-target experiment using the proton and ion LHC beams [6] –

---

<sup>1</sup>P. Ramalhete, [PhD. thesis](#), April 2009.

referred thereafter to as AFTER@LHC. In such collisions, one can investigate specific reactions where one of the colliding particle serves as a (coherent) emitter of a photon and the other serves as a target. Such photon-hadron collisions can be (semi-)exclusive, resulting, for instance, in the sole production of a lepton pair. This process can be used to monitor the experiment luminosity since it mainly comes from the Bethe-Heitler (BH) process [7], whose cross section is well-known. By looking at the target rapidity region, it can also be used to scan the domain of validity of the Equivalent-Photon Approximation (EPA). It can also be used to probe the inner structure of the target, through the interference between the BH process and the Timelike Compton Scattering (TCS) [8–10]. Such an interference – measurable via the analysis of the azimuthal anisotropy – indeed involves contributions from the Generalised Parton Distributions (GPD) [11–18].

The structure of this article is as follows. In section 2, we present the main characteristics of the UPCs and the corresponding photon fluxes in a fixed-target mode on the LHC beams. In section 3, we briefly discuss the cross sections for production of lepton pair via the BH process. In section 4, we discuss how the contribution from TCS can be extracted and how they can help to unravel information about the inner proton structure. In section 5, we briefly discuss the potential competing hadronic process resulting from photon-odderon fusion. Finally, we present our outlooks and conclusions.

## 2 Ultraperipheral collisions in a high-energy fixed-target experiment

### 2.1 Generalities on photon-induced reactions in ultraperipheral collisions

Relativistically moving charged hadrons are accompanied by electromagnetic fields which can effectively be used as quasi-real-photon beams. At very high energies, these photons are energetic enough to initiate hard reactions, just as in lepton-proton colliders.

The virtuality,  $q^2 = -Q^2$ , of these photons is small,  $Q^2 \lesssim 1/R^2$ , where  $R$  is the radius of the charge. More precisely,  $Q \lesssim 0.28$  GeV for protons ( $R \approx 0.7$  fm) and  $Q \lesssim 0.06$  GeV for nuclei ( $R_A \approx 1.2 A^{1/3}$  fm) with a mass number  $A > 16$ . These photons, which are emitted coherently, are almost on mass shell, and their emission can be theoretically treated in the EPA (see *e.g.* [19]).

Seen from a target at rest, the energy of these photons can become significant if the energy of the moving charge, *i.e.* the beam energy, becomes ultra-relativistic, as at the LHC. At rest, the coherent photon cloud of an heavy ion is on the order of 30 MeV. Boosted a few thousand times ( $\gamma_{\text{Pb}} \simeq 2940$ ), these photons have an energy close to 100 GeV in the laboratory frame. It is of course much less than what can be achieved at the LHC in the collider mode, but close to the experimental condition at RHIC with colliding beams of 100 GeV. It is anyhow enough to produce hard dileptons as well as vector mesons.

The energy spectrum of these photons depends on the boost with respect to the observer as well as the impact parameter  $b$  – it is understood that the observer or the probe is outside the charge distribution. Using the EPA method, one gets [20] that the flux as function of the photon momentum  $k$ , of  $b$  and  $\gamma$  (the Lorentz factor of the hadron – or

nucleus – in the frame where  $k$  is measured) reads

$$\frac{dn}{dkd^2b} = \frac{Z^2\alpha_{\text{em}}\omega(b,k)^2}{\pi^2kb^2} \left[ K_1^2(\omega(b,k)) + \frac{1}{\gamma^2} K_0^2(\omega(b,k)) \right], \quad (2.1)$$

where  $\alpha_{\text{em}}$  is the QED coupling,  $Z$  is the nucleus charge,  $\omega(b,k) = kb/\gamma$  and  $K_{1,2}$  are modified Bessel functions of the second kind.

**Table 1:** Relevant parameters for  $AB$  UPCs at AFTER@LHC, at RHIC and at SPS: (i) nucleon-nucleon cms,  $\sqrt{s_{NN}}$  (ii) luminosity,  $\mathcal{L}_{AB}$ , (iii-iv) colliding hadron energies,  $E_{A,B}^{\text{lab}}$ , in the laboratory frame, (v) Lorentz factor between the colliding hadron rest frame and cms,  $\gamma = \sqrt{s_{NN}}/(2m_N)$ , (vi) Lorentz factor between both colliding hadron rest frames,  $\gamma = s_{NN}/(2m_N^2)$ , (vii-viii) inverse of the colliding hadron effective radii (giving the typical photon cloud energy in the emitter rest frame) (ix-x) photon “cutoff energy” in the target (resp. projectile) rest frame,  $E_{\gamma \text{ max}}^{\text{B rest}}$  (resp.  $E_{\gamma \text{ max}}^{\text{A rest}}$ ) (xi-xii) “maximum” photon-nucleon cms energy where  $A$  (resp.  $B$ ) is the photon emitter,  $\sqrt{s_{\gamma N}^{\text{max}}}$  (resp.  $\sqrt{s_{N\gamma}^{\text{max}}}$ ) (xiii) photon “cutoff energy” in the cms,  $E_{\gamma \text{ max}}^{\text{cms}}$ , with both  $A$  and  $B$  emitting a photon coherently (xiv) “maximum” photon-photon cms,  $\sqrt{s_{\gamma\gamma}^{\text{max}}}$ .

| System        | target thickness | $\sqrt{s_{NN}}$ | $\mathcal{L}_{AB}^2$               | $E_A^{\text{lab}}$ | $E_B^{\text{lab}}$ | $\gamma^{\text{cms}}$                     | $\gamma^{A\leftrightarrow B}$        | $\frac{\hbar c}{R_A+R_B}$ | $E_{\gamma \text{ max}}^{A/B \text{ rest}}$ | $\sqrt{s_{\gamma N}^{\text{max}}}$ | $E_{\gamma \text{ max}}^{\text{cms}}$ | $\sqrt{s_{\gamma\gamma}^{\text{max}}}$ |
|---------------|------------------|-----------------|------------------------------------|--------------------|--------------------|---|--------------------------------------|---------------------------|---|------------------------------------|---------------------------------------|--|
|               | (cm)             | (GeV)           | ( $\text{pb}^{-1}\text{yr}^{-1}$ ) | (GeV)              | (GeV)              | $\left(\frac{\sqrt{s_{NN}}}{2m_N}\right)$ | $\left(\frac{s_{NN}}{2m_N^2}\right)$ | (MeV)                     | (GeV)                                       | (GeV)                              | (GeV)                                 | (GeV)                                  |
| AFTER@LHC     |                  |                 |                                    |                    |                    |   |                                      |                           |   |                                    |                                       |  |
| $pp$          | 100              | 115             | $2.0 \times 10^4$                  | 7000               | $m_N$              | 61.0                                      | 7450                                 | 141                       | 1050  | 44                                 | 8.6                                   | 17                                     |
| $p\text{Pb}$  | 1                | 115             | 160                                | 7000               | $m_N$              | 61.0                                      | 7450                                 | 25.3                      | 188   | 19                                 | 1.5                                   | 3.1                                    |
| $pd$          | 100              | 115             | $2.4 \times 10^4$                  | 7000               | $m_N$              | 61.0                                      | 7450                                 | 69.5                      | 517   | 31                                 | 4.2                                   | 8.5                                    |
| $\text{PbPb}$ | 1                | 72              | $7. \times 10^{-3}$                | 2760               | $m_N$              | 38.3                                      | 2940                                 | 13.9                      | 40.7  | 8.8                                | 0.53                                  | 1.1                                    |
| $\text{Pbp}$  | 100              | 72              | 1.1                                | 2760               | $m_N$              | 38.3                                      | 2940                                 | 25.3                      | 74.2  | 12                                 | 0.97                                  | 1.9                                    |
| $\text{Arp}$  | 100              | 77              | 1.1                                | 3150               | $m_N$              | 40.9                                      | 3350                                 | 41.1                      | 138   | 16                                 | 1.7                                   | 3.4                                    |
| $\text{Op}$   | 100              | 81              | 1.1                                | 3500               | $m_N$              | 43.1                                      | 3720                                 | 53.0                      | 197   | 19                                 | 2.3                                   | 4.6                                    |
| RHIC          |                  |                 |                                    |                    |                    |   |                                      |                           |   |                                    |                                       |  |
| $pp$          | n/ap             | 200             | 12                                 | 100                | 100                | 106                                       | 22600                                | 141                       | 3190  | 77                                 | 15                                    | 30                                     |
| $\text{AuAu}$ | n/ap             | 200             | $2.8 \times 10^{-3}$               | 100                | 100                | 106                                       | 22600                                | 14.2                      | 320   | 25                                 | 1.5                                   | 3.0                                    |
| SPS           |                  |                 |                                    |                    |                    |   |                                      |                           |   |                                    |                                       |  |
| $\text{InIn}$ | n/av             | 17              | n/av                               | 160                | $m_N$              | 9.23                                      | 170                                  | 16.9                      | 2.87  | 2.4                                | 0.16                                  | 0.31                                   |
| $\text{PbPb}$ | n/av             | 17              | n/av                               | 160                | $m_N$              | 9.23                                      | 170                                  | 13.9                      | 2.36  | 2.1                                | 0.13                                  | 0.26                                   |

Unless  $b$  is smaller<sup>3</sup> than  $R$ , the strong suppression of the flux by the Bessel functions when  $\omega$  gets of the order of unity implies that  $k$  should be smaller than inverse radius times the Lorentz factor  $\gamma$ . The larger  $\gamma$  is and the smaller the emitter is, the harder the flux is. We also note that the energy spectrum  $kdn/dk$  is constant for  $k/\gamma$  fixed. To fix the idea, one usually considers a maximum photon momentum  $k^{\text{max}} \simeq \frac{\hbar c}{R_{\text{emitter}}}$  below which the emission are likely coherent and therefore characterised by a flux proportional to  $Z^2$ . This

<sup>2</sup>For  $\text{Arp}$  and  $\text{Op}$  luminosity with AFTER@LHC, we conservatively assumed the same extracted flux of  $\text{Ar}$  and  $\text{O}$  as for  $\text{Pb}$ , *i.e.*  $2 \times 10^5$   $\text{Pb/s}$ . See also [6, 21–23]

<sup>3</sup>Otherwise, (i) one cannot consider the entire nucleus charge  $Z$ , (ii) hadronic interactions may be more important than the photon-induced ones, (iii) the probably for the colliding objects to break-up may also be important.

quantity should not thus be considered as a sharp cut-off above which photon emissions are forbidden. If the photon is considered in the hadron cms, one has  $\gamma = \sqrt{s_{NN}}/(2m_N)$  ( $\equiv \gamma^{\text{cms}}$ ). If the photon is considered in the target  $B$  rest frame,  $\gamma = s_{NN}/(2m_N^2)$  ( $\equiv \gamma^{A \rightarrow B}$ ). Table 1 summarises the relevant parameters characterising ultra-peripheral collisions at AFTER@LHC, at RHIC and a SPS in fixed-target mode.

For comparisons with photon-induced reactions in the more conventional lepton-hadron collisions, it is usually more instructive to look at the maximum of the  $\gamma N$  cms energy,  $\sqrt{s_{\gamma N}^{\text{max}}}$ . To do so, we “boost”<sup>4</sup>  $k^{\text{max}}$  in the “target” nucleon rest frame, to obtain  $E_{\gamma \text{ max}}^N \text{ rest} = \gamma^{A \rightarrow B} k^{\text{max}}$ , where  $\sqrt{s_{\gamma p}} = \sqrt{2E_{N \text{ rest}}^{\text{max}} m_N} = \sqrt{s_{NN} k^{\text{max}}/m_N}$ . We note that the photon-energy “cut-off” obtained with these dimensional arguments for Pb $p$ , *i.e.* 74 GeV, is remarkably close to the peak in the energy spectrum obtained using a more realistic model in a recent study of the Bremsstrahlung spectrum of ions in AFTER@LHC [24], *i.e.* 80 GeV.

## 2.2 Photon fluxes

Taking into account the smallest possible impact parameter for a given colliding system,  $pp$ ,  $pA$  or  $AB$ , as well as the charge distribution through a form factor in the proton case, one obtains different formulae for the flux integrated in  $b$ . In fact, the photon fluxes do not formally factorise since  $b_{\text{min}}$  depends on the radius of both colliding objects, except in  $ep$  collisions, where one can reasonably neglect the electron radius.

Along these lines, one should normally have for  $pp$  collisions,  $b_{\text{min}} \simeq 2 \times R_p$ ; for  $pA$  collisions,  $b_{\text{min}} \simeq R_p + R_A$ ; and for  $AB$  collisions  $b_{\text{min}} \simeq R_A + R_B$ . Whereas it is acceptable to approximate  $R_p + R_A$  to  $R_A$ , it does not seem justifiable to use  $R_{\text{Pb}}$  for PbPb collisions, for instance. In addition, in  $pA$  collisions, it is also problematic to use a different  $b_{\text{min}}$  when one considers the proton emission or the ion emission. In both cases, one should use  $R_p + R_A$ , or perhaps  $R_A$ .

Integrating Eq. (2.1) over  $b$ , one has [20]

$$\frac{dn}{dk} = \frac{2Z^2 \alpha_{\text{em}}}{\pi k} \left[ \omega(b_{\text{min}}, k) K_0(\omega(b_{\text{min}}, k)) K_1(\omega(b_{\text{min}}, k)) - \frac{\omega(b_{\text{min}}, k)^2}{2} (K_1^2(\omega(b_{\text{min}}, k)) - K_0^2(\omega(b_{\text{min}}, k))) \right]. \quad (2.2)$$

To avoid any confusion with the choice of the frame, it is useful to work with the momentum fraction or light cone coordinate,  $x_\gamma = k/p_h \simeq k/(\gamma M_N)$ , where  $p_h$  is the momentum of the hadron emitting the photon. One trivially obtains

$$\frac{dn}{dx_\gamma} = \frac{k}{x_\gamma} \frac{dn}{dk} \Big|_{\omega_{pA} = x_\gamma M_p b_{\text{min}}}. \quad (2.3)$$

---

<sup>4</sup>In fact, the procedure looks more as if the emitter is Lorentz contracted as  $1/\gamma$ , rather than the photon momentum boosted. The results are however similar once one considers the emitted photon as slightly off-shell, with a momentum, in the rest frame of the emitter, as  $(k^{\text{max}}, 0, 0, 0)$ .

The relation between the (differential) hadron-hadron cross section,  $(d)\sigma^{h_A h_B}$ , and the (differential) cross section for a photo-hadron scattering ( $h_A$  or  $h_B$ ),  $(d)\sigma^{\gamma h_{A,B}}$ , is naturally given by the following convolution with the photon flux

$$\begin{aligned} d\sigma^{h_A h_B} &= \int dk_\gamma \left( \frac{dn^{h_A}}{dk_\gamma} d\sigma^{\gamma h_B}(s_{\gamma h_B}(k_\gamma)) + \frac{dn^{h_B}}{dk_\gamma} d\sigma^{\gamma h_A}(s_{\gamma h_A}(k_\gamma)) \right) \\ &= \int dx_\gamma \left( \frac{dn^{h_A}}{dx_\gamma} d\sigma^{\gamma h_B}(s_{\gamma h_B}(k_\gamma(x_\gamma))) + \frac{dn^{h_B}}{dx_\gamma} d\sigma^{\gamma h_A}(s_{\gamma h_A}(k_\gamma(x_\gamma))) \right). \end{aligned} \quad (2.4)$$

By analogy with the parton model formulae, one can thus write:

$$\varphi_\gamma(x_\gamma) = \frac{dn}{dx_\gamma}, \quad (2.5)$$

and interpret the latter as an equivalent-photon PDFs off the hadron (or the ions) by leaving the emitter intact.

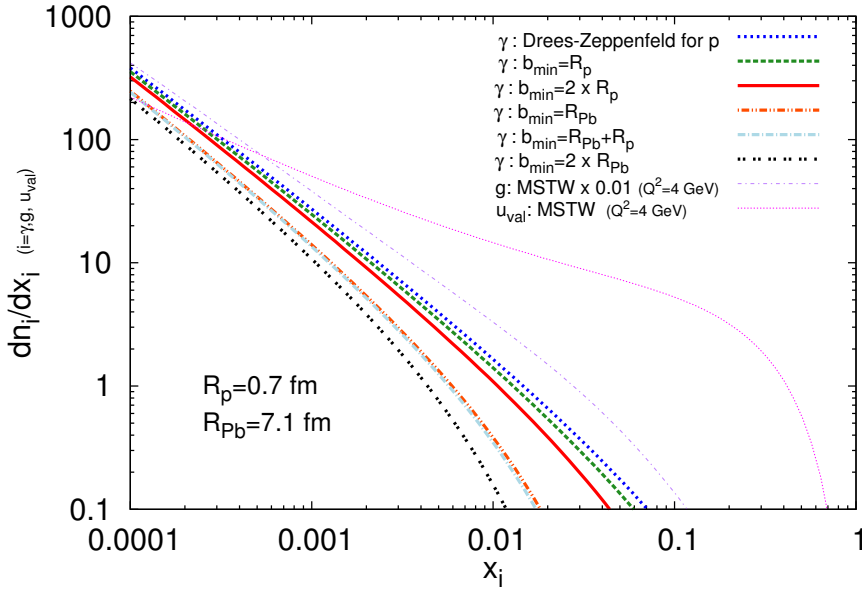


**Figure 1:**  $\frac{dn}{dx}$  for photons from protons (blue dot for Drees-Zeppenfeld, green dash for  $b_{\min} = R_p$  and red solid for  $b_{\min} = 2R_p$ ) and from Pb (orange double dot dash for  $b_{\min} = R_{Pb}$ , light blue dot dash for  $b_{\min} = R_{Pb} + R_p$  and black double dot for  $b_{\min} = 2R_{Pb}$ ) divided by  $Z_{Pb}^2$ . These are compared to the gluon (thin pink long-dash, divided by 100) and  $u$  quark (thin purple dot-dash) MSTW PDF in the proton.

In the case where the emitter is a proton, one could think that it is more accurate to take into account the spatial distribution of the charges through a form factor, which leads [25] to

$$\frac{dn}{dx_\gamma} = \frac{\alpha}{2\pi x_\gamma} \left( 1 + (1 - x_\gamma)^2 \right) \left[ \ln c - \frac{11}{6} + \frac{3}{c} - \frac{3}{2c^2} + \frac{1}{3c^2} \right], \quad (2.6)$$

where  $c = 1 + \frac{0.71 \text{ GeV}^2}{Q_0^2}$ , and  $Q_0^2 = M_p^2 x_\gamma^2$ . This is only strictly relevant for  $ep$  collisions and at rather large  $x_\gamma$ . In  $pp$  or  $pA$  collisions, one indeed needs to take into account the radius of the other colliding object. The impact parameter  $b$  is therefore not getting close to  $R_p$ . We will refer to this choice by ‘‘Drees-Zeppenfeld’’.

Fig. 1 shows a comparison (up to the charge factor  $Z^2$ ) between the equivalent flux from a proton and from a lead ion. For  $x_\gamma < 10^{-3}$ , the spectra show a similar behaviour, with a magnitude differing by less than a factor 2. At larger  $x_\gamma$ , the proton spectrum is clearly harder because of the smaller proton size. This is the expected behaviour.

One could also consider the case where the proton emitting the photon breaks apart. In this situation, the photon is in fact radiated by the quarks and the corresponding photon PDF can then be approximated by [26]

$$\varphi_\gamma^{\text{break-up}}(x, Q^2) = \frac{\alpha}{2\pi} \log \frac{Q^2}{Q_0^2} \sum_q \int_x^1 \frac{dy}{y} P_{\gamma q}(x/y) [q(y, Q^2) + \bar{q}(y, Q^2)], \quad (2.7)$$

with  $P_{\gamma q}(z) = e_q^2 (1 + (1-z)^2)/z$ ,  $Q_0^2$  is an energy cut-off, and  $q(x, Q^2)$  is the quark PDFs in the proton. We will not consider this possibility further in this study, although such a process could contribute to the semi-exclusive case with still a large rapidity gap between the dilepton and the proton emitter. Another possibility, which we will discuss in section 5 is to have an elastic *hadronic* reaction via the exchange of a pomeron (or possibly an odderon).

## 2.3 Fluxes and the rapidity dependence of the produced particles

### 2.3.1 Single-photon case

If we consider the *total* cross section,  $\sigma^{\gamma h}$ , to photo-produce a particle of mass  $Q$ , we note that it can only be function of  $s_{\gamma h}$  and  $Q^2$  since it is already integrated on the final state variables. However, nothing prevents us to perform a change of variable in Eq. (2.4) from  $k_\gamma$  to a final state variable of the  $\gamma$ -hadron process, for instance the rapidity  $y$  of the produced particle, keeping the other fixed<sup>5</sup>. By momentum conservation,  $y$  would enter<sup>6</sup> via  $k_\gamma(y)$  in  $s_{\gamma h}$

Indeed, in our case, it is clearly instructive, in order to understand where the produced particle by photon-induced collisions fly, to consider the flux as a function of the particle rapidity  $y$  in the laboratory frame. For instance, we anticipate [6] that rapidities (in the laboratory frame) from -4 to +1 should be accessible.

For fixed  $q_T$  and  $Q^2$ ,  $k_\gamma(y)$  is also fixed. From Eq. (2.4), one trivially obtains

$$\begin{aligned} d\sigma^{hh} &= \int dk_\gamma \left( \frac{dn^{h_A}}{dk_\gamma} d\sigma^{\gamma h_B}(s_{\gamma h_B}(k_\gamma)) + \frac{dn^{h_B}}{dk_\gamma} d\sigma^{\gamma h_A}(s_{\gamma h_A}(k_\gamma)) \right) \\ &= \int dy \left( \frac{dn^{h_A}}{dy} d\sigma^{\gamma h_B}(s_{\gamma h_B}^A(y)) + \frac{dn^{h_B}}{dy} d\sigma^{\gamma h_A}(s_{\gamma h_A}^B(y)) \right), \end{aligned} \quad (2.8)$$

<sup>5</sup>In the following, we denote the 4-momentum of this particle  $q = (q_0, \vec{q}_T, q_z)$  and  $q_T = |\vec{q}_T|$ .

<sup>6</sup>Defining  $x_\gamma = s_{\gamma h}/s$ , one indeed gets  $x_\gamma = x_\gamma(y, q_T^2, Q, \epsilon)$  where  $\epsilon = \pm 1$  when the projectile (target) is the photon emitter. See the appendix A for details.

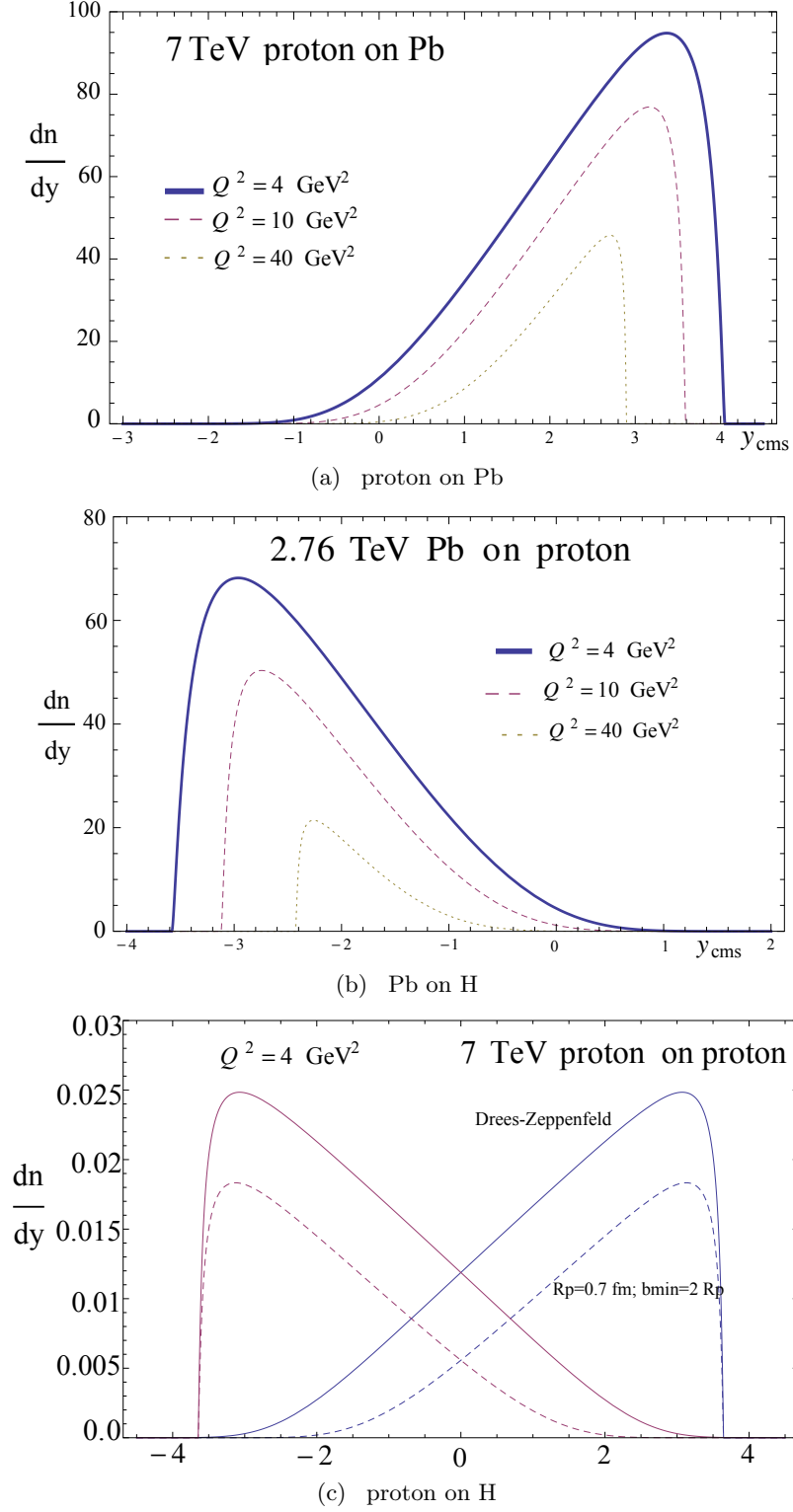


**Figure 2:**  $\frac{dn}{dy}$  for the proton run on Pb nucleon target (a), and for Pb run on H target (b), and (c) for p-p run. The flux is calculated for the specified  $Q^2$  at  $q_T = 0$  (e.g.  $t = t_0$ ).



where  $s_{\gamma h(B,A)}^{(A,B)}(y) \equiv s_{\gamma h(B,A)}(k_{\gamma \text{ from (A,B)}}(y))$  and therefore

$$\frac{d\sigma^{hh}}{dy} = \frac{dn^{h_A}}{dy} d\sigma^{\gamma h_B}(s_{\gamma h_B}^A(y)) + \frac{dn^{h_B}}{dy} d\sigma^{\gamma h_A}(s_{\gamma h_A}^B(y)). \quad (2.9)$$

We therefore find it instructive to plot  $\frac{dn}{dy}$  (for fixed  $q_T$  and  $Q^2$ ) for different configurations: Fig. 2a shows the case of 7 TeV protons on lead, the lead being the photon emitter; Fig. 2b shows the case of 2.76 TeV lead on protons, the lead being the photon emitter<sup>7</sup>; Fig. 2c shows the case of 7 TeV protons on proton (i.e. hydrogen), where both can be the photon emitter (note that the corresponding fluxes cannot simply be summed).

In the first case (Fig. 2a), the flux is maximum in the forward region, which corresponds to a soft (coherent) emission by the lead target. In general, the particle tends to be emitted in the ‘‘hadron-receiver’’ region since the photon momentum is very small (here  $y_{\text{receiver=beam}} = 4.8$ ). To be more precise, the boost – or rapidity difference  $\Delta y$  – between the photon-hadron and hadron-hadron cms,  $\Delta y_{h_A h_B}^{\gamma h_{A,B}} = y_{\text{cms}}^{h_A h_B} - y_{\text{cms}}^{\gamma h_{A,B}}$ , is simply related to the photon momentum fraction via

$$\Delta y_{h_A h_B}^{\gamma h_{A,B}} = -\epsilon \frac{1}{2} \ln x_{\gamma}, \quad (2.10)$$

In order to produce a particle of mass  $Q$  at threshold<sup>8</sup> in a photon-hadron collision at  $\sqrt{s_{\gamma h}}$  resulting from a hadron-hadron UPC at  $\sqrt{s_{NN}}$ , one approximately has  $x_{\gamma} \simeq Q^2/s_{NN}$ . At AFTER@LHC, for  $Q^2 = 4 \text{ GeV}^2$ ,  $x_{\gamma} = 3 \times 10^{-4}$ , which gives  $\Delta y_{h_A h_B}^{\gamma h_{A,B}} \simeq -4$ . This explains the maximum at  $y_{\text{cms}} \simeq 4$  of the solid line of Fig. 2a.

If the emission is too soft, there is simply not enough energy to create a particle of a given mass,  $Q$ , – this explains why the curve for  $Q^2 = 4(40) \text{ GeV}^2$  drops sharply at  $y_{\text{cms}} \simeq 4(3)$ . In the second case (Fig. 2b), the flux is the highest in the opposite direction where soft photons are emitted by the lead projectile. Since the lead beam energy is lower ( $y_{\text{beam}} = 4.2$ ) and the energy cut-off smaller, the particle is less backward than it is forward in the first case. In the third case (Fig. 2c), both proton can emit. The behaviour is similar to (a) and (b), but for a lower value due to the absence of the factor  $Z^2$ . It is however harder in the forward (backward) region for a projectile (target) proton emitter – note that the flux in the tail is still nonzero at  $y$  down to  $\pm 3$ . This mirrors the possibility for harder photon (up to  $x_{\gamma} \simeq 0.1$ ) emission from a proton compared to a larger nucleus. The solid and dashed curves on Fig. 2c refer to two different fluxes: Drees-Zeppenfeld as in  $ep$  collisions (solid) and  $b_{\text{min}} = 2 \times R_p$  (dashed).

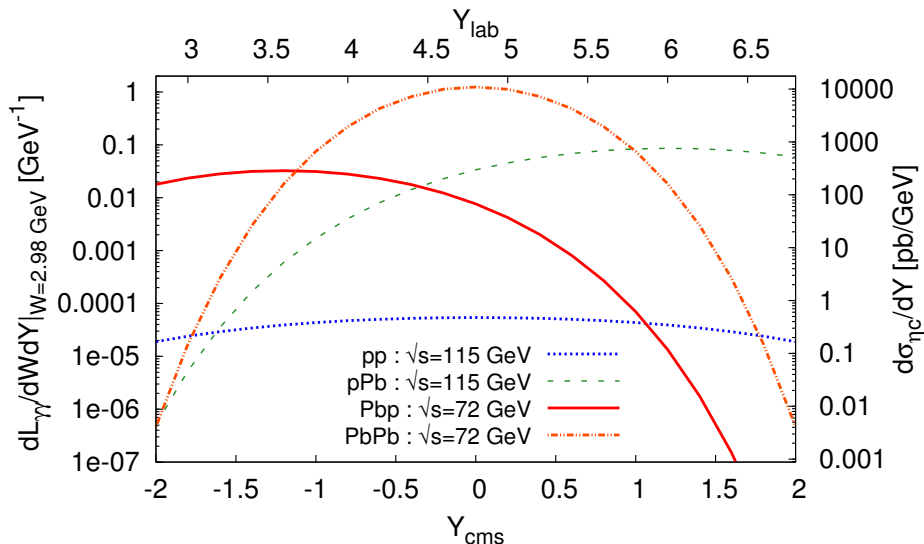
The advantage offered by the fixed-target mode is therefore obvious when the emitter is the projectile. In such a case, the large rapidity differences between the photon-hadron and hadron-hadron cms and that between the hadron-hadron cms and the laboratory frame nearly cancel. This results in the production of the particle at slightly positive rapidities which are easily covered by typical detectors.

<sup>7</sup>In this case, as for (a), the photon emission by a lead ion can, in principle, be tagged with a neutron emission. In addition, the probability for the proton to be the emitter is, in practice, negligible ( $Z^2$  suppressed at the same  $|y_{\text{cms}}|$ ). We therefore do not show the curve for this possibility.

<sup>8</sup>*i.e.* at rest in the photon-hadron cms.

### 2.3.2 Double-photon case

Obviously, one can also consider UPC where both colliding hadrons radiate a photon. This is expected to be the dominant reaction at work in dilepton production,  $AA' \rightarrow A\ell^+\ell^-A'$ ,  $\text{PbH} \rightarrow \text{Pb}\ell^+\ell^- \text{H}$ ,  $p\text{Pb} \rightarrow p\ell^+\ell^- \text{Pb}$  or  $pp' \rightarrow p\ell^+\ell^- p'$ , via  $\gamma\gamma \rightarrow \ell^+\ell^-$  (see Fig. 4a), that is the BH process. Combining the fluxes from both hadrons, one can derive a joint photon flux or  $\gamma\gamma$  luminosity as function of their invariant mass,  $\sqrt{s_{\gamma\gamma}}$  or  $W$ , and rapidity  $Y$ , as it is usually done for  $gg$  luminosity at the LHC to discuss  $H^0$  production rates, for instance.



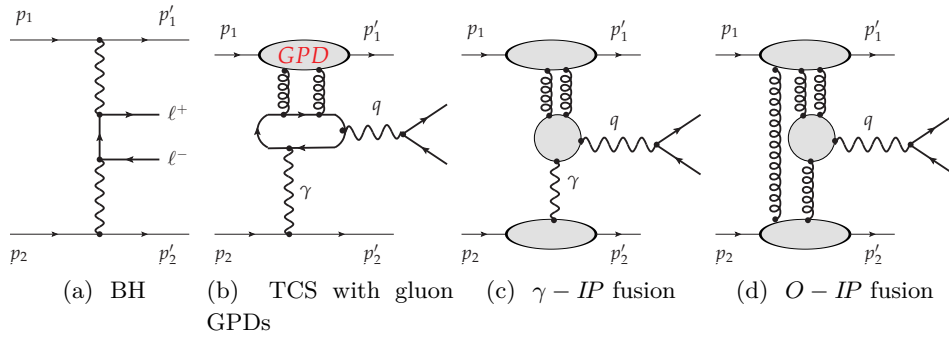
**Figure 3:**  $\frac{dL_{\gamma\gamma}}{dWdY}\Big|_{W=m_{\eta_c}}$  (and  $\frac{d\sigma_{\eta_c}}{dY}$ ) as a function of the rapidity, in the hadron-hadron cms (lower  $x$ -axis) and in the laboratory frame (upper  $x$ -axis)<sup>9</sup>.

Fig. 3 shows the rapidity dependence of  $\gamma\gamma$  luminosity in the hadron-hadron cms at a fixed  $W$ , obtained from of Eqs. 42, 43, 50, 51 and 52 of [27] with numerical integrations on the impact parameters. In the case of the BH process discussed in detail in the next section, the invariant mass of the pair is that one the dilepton. One observes that the maxima in the  $\text{Pbp}$  and  $p\text{Pb}$  fluxes occur at respectively backward (forward) rapidities because the photon spectrum from the proton is harder than that from the ion.

### 3 Lepton-pair production: energy, invariant-mass, rapidity and transverse-momentum dependencies

We now discuss in more details the dominant process involved in lepton-pair production that is BH from  $\gamma\gamma \rightarrow \ell^+\ell^-$  (Fig. 4a) in hadron-hadron collisions.

<sup>9</sup>The reason why we took  $W = m_{\eta_c} = 2.98$  GeV for this example will become clear in the next section.



**Figure 4:** Feynman graphs representing the scattering of two hadrons of momentum  $p_1$  and  $p_2$  remaining intact with final state momenta  $p'_1$  and  $p'_2$  producing a lepton pair via (a) the BH process by photon-photon fusion, (b) via TCS described in terms of a GPD (here the gluon one), (c) via photon-pomeron fusion represented by the minimal number of gluon exchanges and (d) via odderon-pomeron fusion also represented with the minimal number of gluon exchanges.

| System   | $pp$  |       | $pPb$ |     | Pbp |     | PbPb |      |
|--|-------|-------|-------|-----|-----|-----|------|------|
| $\sqrt{s_{NN}}$ [GeV]  | 115   |       | 115   |     | 72  |     | 72   |      |
|  | BW    | SL    | BW    | SL  | BW  | SL  | BW   | S    |
| $\frac{d\sigma_{\ell\ell}(Q=2 \text{ GeV})}{dQ}$ [nb/GeV]  | 0.14  | 0.15  | 200   | 210 | 77  | 84  | 7000 | 7100 |
| $\frac{d\sigma_{\ell\ell}(Q=2 \text{ GeV}, y_{\text{cms}}^{\ell^+\ell^-}=0)}{dQ dy_{\text{cms}}^{\ell\ell}}$ [nb/GeV]    | 0.039 | 0.038 | 39    | 45  | 14  | 16  | 5500 | 5600 |
| $\frac{d\sigma_{\ell\ell}(Q=2.98 \text{ GeV})}{dQ}$ [nb/GeV]   | 0.03  | 0.031 | 32    | 34  | 9.7 | 11  | 230  | 250  |
| $\frac{d\sigma_{\ell\ell}(Q=2.98 \text{ GeV}, y_{\text{cms}}^{\ell^+\ell^-}=0)}{dQ dy_{\text{cms}}^{\ell\ell}}$ [nb/GeV] | 0.009 | 0.009 | 5.7   | 6.5 | 1.3 | 1.6 | 200  | 210  |

**Table 2:** BH differential cross section for fixed dilepton masses integrated (or not) on  $y_{\text{cms}}^{\ell\ell}$ . “BW” denotes Breit-Wheeler and “SL” denotes STARLIGHT.

### 3.1 Total cross section and for fixed $Q$

The total cross section for dimuon production by two heavy and charged particles is well known and can readily be computed from the analytical formula of Racah [28]. At  $\sqrt{s} = 115$  GeV, one gets 15.0 nb for  $pp$  collisions, to be compared with 16.5 nb with the STARLIGHT Monte Carlo code<sup>10</sup>. The corresponding cross section for  $pPb$  is simply obtained by multiplying by  $Z^2$ , *i.e.* 100  $\mu\text{b}$ . In this case, it is assumed that the particles are point-like. STARLIGHT rather gives 36  $\mu\text{b}$ .

We are however interested in the differential cross sections for particular values of the dilepton invariant mass,  $Q$ ; muon pairs produced at  $Q \gtrsim 2m_\mu$  are usually difficult to study since the muons have small transverse momenta. Such a cross section can easily be obtained by combining two EPA photon fluxes as done to obtain  $\frac{dL_{\gamma\gamma}}{dW dY}$  and then by integrating over

<sup>10</sup>STARLIGHT website.

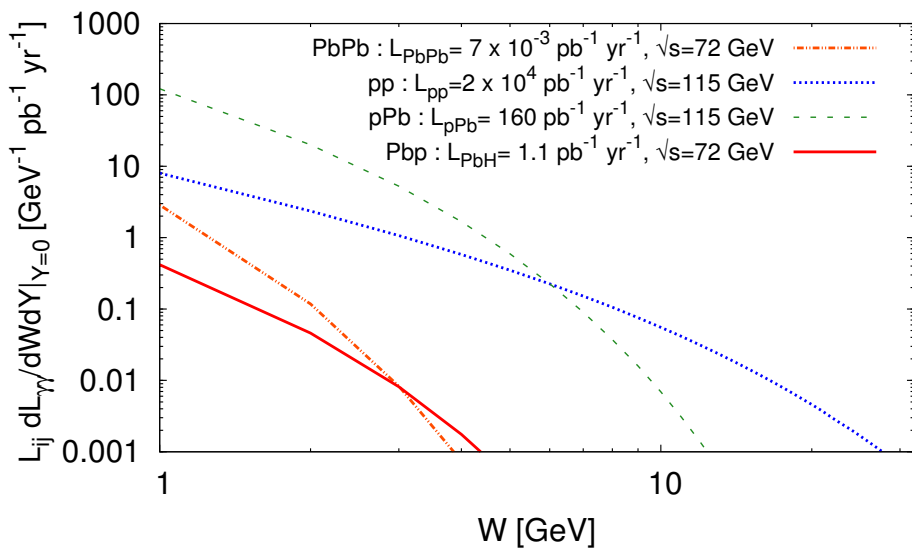


**Figure 5:**  $\mathcal{L}_{ij} \times \frac{dL_{\gamma\gamma}}{dW}$  from protons and from Pb in  $pp$ ,  $pPb$ ,  $PbH$  and  $PbPb$  collisions (see Table 1) as a function of the invariant mass of the photon pair,  $W$ , at  $Y_{\text{cms}}=0$  of the  $\gamma\gamma$  pair (or of the to-be produced dilepton).

Y. One then convolve it with the Breit-Wheeler formula [29]:

$$\sigma_{\ell\ell}^{\gamma\gamma}(Q^2) = \frac{4\pi\alpha^2}{Q^2} \left[ \left( 2 + \frac{8m_\ell^2}{Q^2} - \frac{16m_\ell^4}{Q^4} \right) \ln \frac{Q + \sqrt{Q^2 - 4m_\ell^2}}{2m_\ell} - \sqrt{1 - \frac{4m_\ell^2}{Q^2}} \left( 1 + \frac{4m_\ell^2}{Q^2} \right) \right]. \quad (3.1)$$

We have checked that we obtained the same result as STARLIGHT for dimuon production, for instance for  $Q = (2, 2.98)$  GeV for  $pp$  and  $pPb$  collisions at  $\sqrt{s_{NN}} = 115$  GeV, as well as for  $Pbp$  and  $PbPb$  collisions at  $\sqrt{s_{NN}} = 72$  GeV, up to the uncertainty attached to the value taken for the nucleus radius, see the first and third rows of results on Table 2.

One readily obtains the rapidity dependence of the differential cross section, by simply using  $\frac{dL_{\gamma\gamma}}{dW dY} \Big|_{W=Q, Y=y_{\text{cms}}^{\ell\ell}}$ . We already discussed it on Fig. 3. The  $\gamma\gamma$  luminosity at a fixed cms rapidity of the photon pair,  $Y_{\text{cms}}$  (or equivalently  $y_{\text{cms}}^{\ell\ell}$ ), is plotted as a function of  $W$  on Fig. 5 namely at  $Y_{\text{cms}} = 0$  for  $pp$ ,  $pPb$ ,  $Pbp$  and  $PbPb$  collisions; it is multiplied by the corresponding hadron yearly luminosity denoted  $\mathcal{L}_{ij}$ . Just as for the rapidity integrated results, both methods agree for  $y_{\text{cms}}^{\ell\ell} = 0$  as it should be, see the second and fourth rows of results on Table 2.

Knowing  $\frac{dL_{\gamma\gamma}}{dW dY}$ , one can also obtain the production cross section for a scalar or tensor quarkonium,  $Q$  provided that we know its partial width into a photon pair,  $\Gamma_{\gamma\gamma}$ :

$$\frac{d\sigma_Q^{h_A h_B}}{dY_Q} \stackrel{\gamma\gamma \rightarrow Q}{=} 8\pi^2 (2J_Q + 1) \frac{\Gamma_{\gamma\gamma}}{2M_Q^2} \frac{dL_{\gamma\gamma}}{dW dY} \Big|_{W=M_Q, Y=Y_Q}. \quad (3.2)$$

From  $\Gamma_{\gamma\gamma}^{\eta_c} = 5.1 \times 10^{-6}$  GeV and  $\Gamma_{\gamma\gamma}^{\chi_{c2}} = 5.3 \times 10^{-7}$  GeV [30], one gets  $\sigma_{\gamma\gamma}^{\eta_c} = 8.8$  nb and  $\sigma_{\gamma\gamma}^{\chi_{c2}} = 3.2$  nb. The rapidity dependence of this cross section is thus up to a constant factor

that of the joint flux at the corresponding<sup>11</sup>  $W$  (see Fig. 3). In particular, for  $pp$  ( $p\text{Pb}$ ) collisions at  $\sqrt{s_{NN}} = 115$  GeV, the  $\eta_c$  cross sections at  $y = 0$  in the hadron-hadron cms are 0.5 pb (0.4 nb) and for  $\text{Pb}p$  ( $\text{PbPb}$ ) collisions at  $\sqrt{s_{NN}} = 72$  GeV, 67 pb (11 nb). With the yearly luminosities in Table 1, one can respectively expect  $10^4$ ,  $1.8 \times 10^6$ , 74 and 80  $\eta_c$  per year.

At this point, two remarks are in order. First, we stress that although,  $m_{\eta_c}$  is above the energy “cut-off” showed in Table 1 for the systems  $p\text{Pb}$ ,  $\text{Pb}p$  and  $\text{PbPb}$ , the rates are nonzero using realistic photon fluxes. Second, our result for  $pp$  collisions is 2-3 times below that recently derived by Goncalves and Sauter [31]. We attribute this difference to the fact that they used the Drees and Zeppenfeld photon flux, which is precisely twice larger than that derived with  $b > 2R_p$  at  $x_\gamma \simeq \sqrt{s}/m_{\eta_c} \simeq 0.025$  (see Fig. 1). As we noted above, the former should only strictly be used for  $ep$  collisions. Such a difference only arises at ‘low’ hadron-hadron cms energies which correspond to  $x_\gamma$  on the order of  $10^{-2}$  and above. A measurement of the  $\eta_c$  or  $\chi_{c2}$  cross section in exclusive  $pp$  collisions at AFTER@LHC is therefore ideal to tell which choice is the most appropriate.

### 3.2 Production at nonzero transverse momenta

If we prefer to look at dileptons produced in reactions characterised by a momentum transfer squared of one emitter,  $|t|$ , up to  $1 \text{ GeV}^2$ , which results in a measurable transverse momentum,  $q_T$ , of the dilepton, it may be more suitable to treat the photon emission using a nucleon form factor<sup>12</sup>. By construction, the off-shellness of this photon cannot be neglected. This amounts to consider the process photoproduction,  $\gamma p \rightarrow \ell^+ \ell^- p$ , where the beam<sup>13</sup> photon flux is still treated in the EPA approximation and the effect of the form factor embedded in the photoproduction cross section.

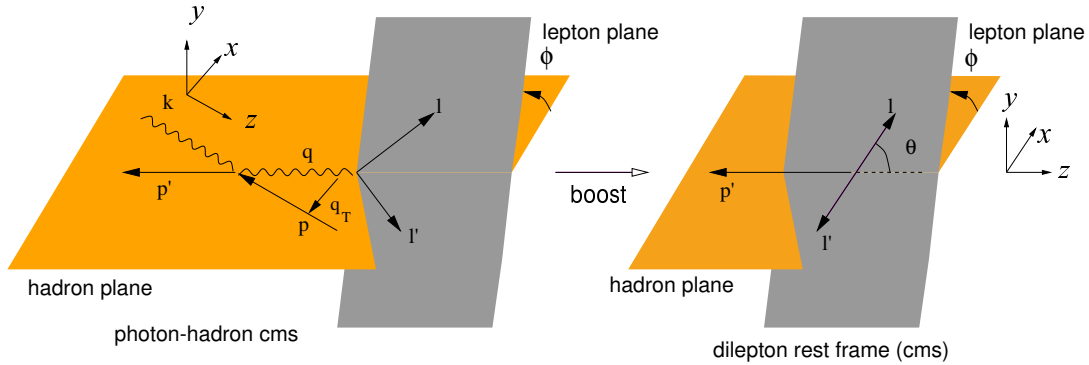


**Figure 6:** Definition of the kinematical variables in  $\gamma(k)h(p) \rightarrow \ell^+(l')\ell^-(l)p(p')$  in particular the angles  $\theta$  and  $\phi$  attached to the  $\ell^-$ .

Following [8], this  $\gamma h$  differential cross section for an unpolarised target to be convoluted with the beam photon flux (provided that  $\sin \theta \gg m_\ell/Q$ ) reads

<sup>11</sup>Hence our choice of  $W = m_{\eta_c} = 2.98$  GeV in Fig. 5.

<sup>12</sup>In the nuclear case, such a configuration is admittedly much suppressed.

<sup>13</sup>The term “beam” may be improper in the fixed-target case since this photon can very well be emitted by a nucleon or nucleus in the target; this is particularly true for  $p\text{Pb}$  collisions.

$$\begin{aligned} \frac{d\sigma_{\ell\ell}^{\gamma h \text{BH}}}{dQ^2 dq_T^2 d\cos\theta d\phi}(y_{\text{cms}}^{\ell\ell}) &\approx J \frac{\alpha_{em}^3}{2\pi s_{\gamma h}^2} \frac{1}{-t} \frac{1 + \cos^2\theta}{\sin^2\theta} \\ &\times \left[ \left( F_1^2(t) - \frac{t}{4M_N^2} F_2^2(t) \right) \frac{2(s_{\gamma h} - M_N^2)^2}{Q^4} \frac{q_T^2}{-t} + (F_1(t) + F_2(t))^2 \right] \Bigg|_{t=t(y_{\text{cms}}^{\ell\ell}, q_T^2, Q, \epsilon)}, \end{aligned} \quad (3.3)$$

where  $F_{1,2}$  are respectively the Dirac and Pauli form factors evaluated at  $t = (p - p')^2 = (k - q)^2$ , the quantity  $\epsilon$  and procedure to obtain  $t(y_{\text{cms}}^{\ell\ell}, q_T^2, Q, \epsilon)$  and  $J$  (the Jacobian to change from  $t$  to  $q_T^2$ ) are explained in the appendix A. The  $\theta$  and  $\phi$  angles are defined as on Fig. 6. The apparent divergence at  $\theta \rightarrow 0$  is regulated when the lepton mass is kept, just as in the Breit-Wheeler equation, Eq. (3.1), which is logarithmically divergent for  $m_\ell \rightarrow 0$ . We note that  $\theta$  – the polar angle of the lepton – which is defined in the rest frame of the dilepton, can only be approximately related to the (pseudo)-rapidity of the lepton in the cms frame for  $y_{\text{cms}}^{\ell\ell} \simeq 0$  and  $q_T \ll Q$ . In such a case, the particular configuration  $\theta \rightarrow \pi/2$  corresponds to  $y_{\text{cms}}^\ell \simeq \eta_{\text{cms}}^\ell \simeq 0$  which falls into the acceptance of a detector like LHCb and ALICE (with Pb beams). Using Eq. (2.9), one then obtains  $d\sigma_{\ell\ell}^{hh \text{BH}} / (dQ^2 dq_T^2 d\cos\theta d\phi dy_{\text{cms}}^{\ell\ell})$ .

#### 4 Timelike compton scattering or exclusive photoproduction of a dilepton

The process of the lepton-pair production in ultraperipheral collisions may also be used to investigate hadron structure in terms of GPDs through the measurement of the contribution of the TCS process, Fig. 4b, to the cross section. Although the BH amplitude squared is much larger than the TCS one, it is possible to study the interference term between TCS and BH processes, which may be projected out through the analysis of the angular distribution of the produced leptons [8] and which depends on the GPDs. The interference term of the differential cross section is given by:

$$\begin{aligned} \frac{d\sigma_{\ell\ell}^{\gamma h \text{INT}}}{dQ^2 dt d\cos\theta d\phi} &\approx -\frac{\alpha_{em}^3}{4\pi s_{\gamma h}^2} \frac{\sqrt{t_0 - t}}{-tQ} \frac{\sqrt{1 - \eta^2}}{\eta} \left( \cos\phi \frac{1 + \cos^2\theta}{\sin\theta} \right) \\ &\times \text{Re} \left[ F_1(t) \mathcal{H}(\eta, t) - \eta(F_1(t) + F_2(t)) \tilde{\mathcal{H}}(\eta, t) - \frac{t}{4M^2} F_2(t) \mathcal{E}(\eta, t) \right], \end{aligned} \quad (4.1)$$

where we have neglected lepton mass and assumed that  $s_{\gamma h}, Q^2 \gg t, M_N^2$ . The variable  $\eta$  called *skewedness* is given by:

$$\eta = \frac{Q^2}{2s_{\gamma h} - Q^2}, \quad (4.2)$$

and  $t_0$  is maximal value of squared momentum transfer  $t$  reached at  $q_T = 0$ , and is equal  $t_0 = -4M^2 \frac{\eta^2}{1 - \eta^2}$  up to corrections in  $1/Q^2$ . The functions  $\mathcal{H}(\eta, t)$ ,  $\tilde{\mathcal{H}}(\eta, t)$  and  $\mathcal{E}(\eta, t)$  are the well known Compton form factors. These involve the GPD  $H$ ,  $\tilde{H}$  and  $E$  (as defined in [15])

respectively through a convolution with the hard-scattering kernels  $T_{\{H,\tilde{H},E\}}^{q,g}$  computed at a given order in  $\alpha_s$ :

$$\{\mathcal{H}, \tilde{\mathcal{H}}, \mathcal{E}\}(\eta, t) = \int_{-1}^1 dx \left[ \sum_q T_{\{H,\tilde{H},E\}}^q(x, \eta) \{H^q, \tilde{H}^q, E^q\}(x, \eta, t) + T_{\{H,\tilde{H},E\}}^g(x, \eta) \{H^g, \tilde{H}^g, E^g\}(x, \eta, t) \right]. \quad (4.3)$$

The expression for the kernels  $T_{\{H,\tilde{H},E\}}$  at LO are given in the appendix B. The Next-to-Leading Order (NLO) hard-scattering kernel<sup>14</sup>, which we use here, can be found in [9, 32].

To advocate that the TCS measurement is feasible in the AFTER kinematics, we present phenomenological predictions making use of two GPD models through double distributions [13]: the first is based on the Goloskokov-Kroll (GK) model based on fits of meson electroproduction data and the second is a model using MSTW8 parton distribution function with a simple factorised  $t$  dependence, referred to as G-MSTW (for a detailed description see [10]).

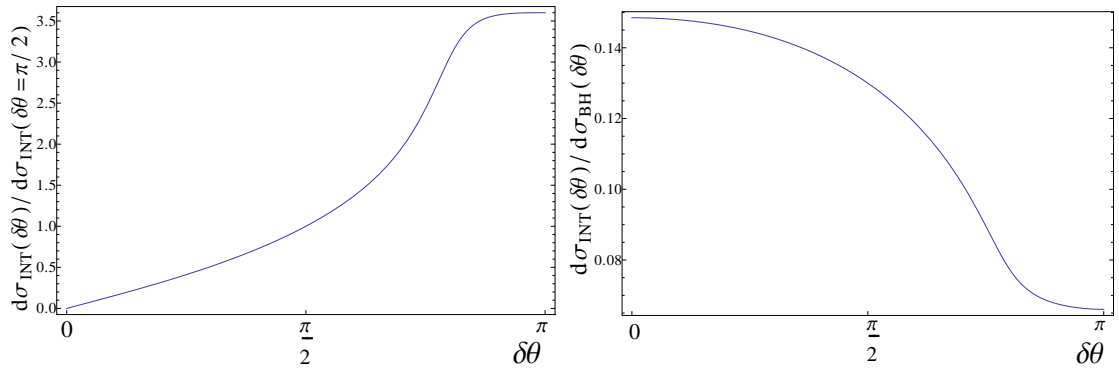


**Figure 7:** (left)  $\frac{d\sigma_{\text{INT}}(\delta\theta)/d\sigma_{\text{INT}}(\delta\theta = \pi/2)}{d\sigma_{\text{INT}}(\delta\theta)/d\sigma_{\text{INT}}(\delta\theta = \pi/2)}$ , (right)  $\frac{d\sigma_{\text{INT}}(\delta\theta)/d\sigma_{\text{BH}}(\delta\theta)}{d\sigma_{\text{INT}}(\delta\theta)/d\sigma_{\text{BH}}(\delta\theta)}$  for the model KG for  $Q^2 = 4 \text{ GeV}^2$ ,  $t = -0.1 \text{ GeV}^2$ , and  $\phi = 0$  for proton run on Pb, integrated over  $\theta \in (\pi/4, 3\pi/4)$  and for  $y = 0$  at NLO.

Comparing the  $\phi$  dependence in Eq. (3.3) to that in Eq. (4.1), one directly sees that one can project out the interference term and eliminate the unwanted BH background by integrating the differential cross section over  $\phi$  with the weight  $\cos \phi$ . To avoid the limit  $\theta \rightarrow 0$  where the BH signal gets very large, one can integrate over  $\theta$  symmetrically around  $\pi/2$  up to a value which depends on the size of the interference. Varying the limits of integration in  $\theta$  according to

$$\theta \in \left( \frac{\pi - \delta\theta}{2}, \frac{\pi + \delta\theta}{2} \right), \quad (4.4)$$

results in the change of the strength of the interference BH-TCS with respect to the BH cross section shown on Fig. 7. On the left panel, we show the ratio of the the integral of

<sup>14</sup>As done in [9], we set  $\mu_R = \mu_F = Q$  in the hard-scattering kernel and, as for other similar phenomenological analyses, the GPDs are not evolved. In the case of the G-MSTW model, the GPDs can be made  $\mu_F$  dependent through the evolution of the input PDFs.

the interference BH-TCS for a given  $\delta\theta$  normalised to that for  $\delta\theta = \pi/2$ . We see that for  $\delta\theta$  close to  $\pi$  the ratio of the integrals of the interference stops increasing. In any case, in this limit, as we present on the right panel, the ratio of the integral of the interference term to the BH one gets very small because the BH cross section gets large<sup>15</sup>. In other words, there is no specific reason to take  $\delta\theta$  much larger than  $\pi/2$ ; below this value the magnitude of the interference term is close to 10 % of the BH term.

One can then combine the  $\gamma h$  cross section with the photon flux as a function of the dilepton rapidity at a fixed  $t$  to get the interference part of 5-fold hadron-hadron differential cross section. Defining the integration region as

$$\int_{\Omega} d^5 F \equiv \int_{\pi/4}^{3\pi/4} d\theta \int_0^{2\pi} d\phi \int_{-2.5}^0 dy \int_0^{0.25} dq_T^2 \int_{1.5}^3 dQ, \quad (4.5)$$

the BH cross section from a 7 TeV proton beam on a Pb target is

$$\sigma_{\text{BH}}^{\text{pPb}} = \int_{\Omega} d^5 F \frac{d\sigma_{\text{BH}}}{dQ dq_T^2 dy d\theta d\phi} = 1940 \text{ pb}, \quad (4.6)$$

which, for a luminosity of  $0.16 \text{ fb}^{-1} \text{ yr}^{-1}$ , gives about  $3 \cdot 10^5$  events per year. In the case of a H target, one has

$$\sigma_{\text{BH}}^{\text{pH}} = \int_{\Omega} d^5 F \frac{d\sigma_{\text{BH}}}{dQ dq_T^2 dy d\theta d\phi} = 7.1 \text{ pb}, \quad (4.7)$$

which, for a luminosity  $= 20 \text{ fb}^{-1} \text{ yr}^{-1}$ , gives  $1.4 \cdot 10^5$  events per year for a 100 cm liquid-hydrogen target. Finally, for Pb on H, one has

$$\sigma_{\text{BH}}^{\text{PbH}} = \int_{\Omega} d^5 F \frac{d\sigma_{\text{BH}}}{dQ dq_T^2 dy d\theta d\phi} = 5500 \text{ pb}, \quad (4.8)$$

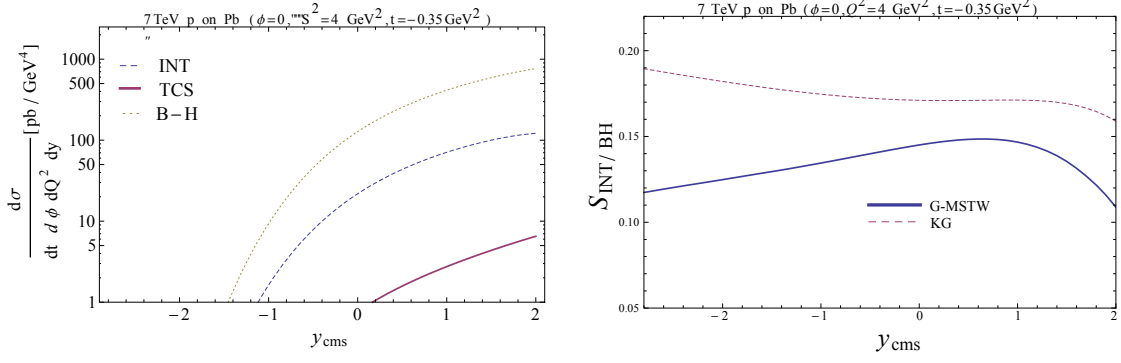
which, for a luminosity  $= 11 \text{ nb}^{-1} \text{ yr}^{-1}$ , gives  $6 \cdot 10^3$  events per year for a 100 cm liquid-hydrogen target. As aforementioned, we do not consider the case where the nucleus is emitter with a  $|t|$  of a few hundred  $\text{MeV}^2$  which should be treated with nucleus form factors and nuclear GPDs. With a magnitude of 10 % for the interference term, the azimuthal modulation should be observable in the 3 cases.

On the Fig. 8, we show the magnitude of the 3 terms as function of the rapidity as well as the relative magnitude of the interference term with respect to the BH one for three cases of collisions (a) proton beam on a Pb target, (b) Pb beam on a H target, (c) proton beam on a H target. On the left panels, we present the rapidity dependence of the BH, TCS and BH-TCS terms of differential cross sections  $\frac{d\sigma}{dy dQ^2 dt d\phi}$  evaluated at  $Q^2 = 4 \text{ GeV}^2$ ,  $t = -0.35 \text{ GeV}^2$  and  $\phi = 0$  and integrated over  $\theta \in (\pi/4, 3\pi/4)$  for the GK model. On the right panels, we show the ratio of the interference signal to the BH for the GK and G-MSTW model. We see that for all cases the signal to the background ratio is around 10-15%.

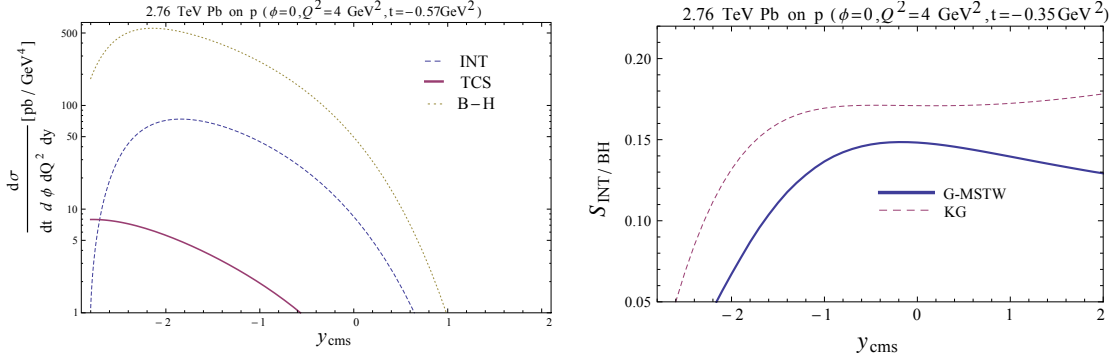
---

<sup>15</sup>In one neglects the lepton, it even diverges.

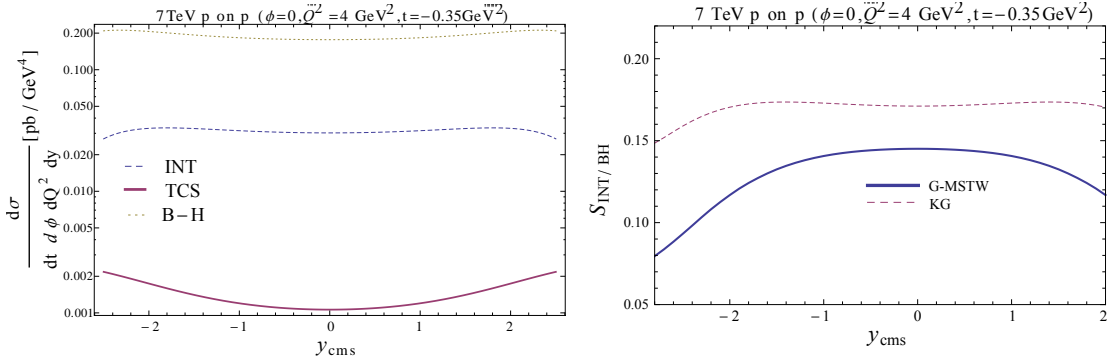




(a) 7 TeV  $p$  on Pb target



(b) 2.76 TeV Pb on H target



(c) 7 TeV  $p$  on H target

**Figure 8:** (Left) Differential cross section  $\frac{d\sigma}{dy dt d\phi dQ^2}$  for the KG model for  $Q^2 = 4 \text{ GeV}^2$ ,  $t = -0.35 \text{ GeV}^2$  and  $\phi = 0$  integrated over  $\theta \in (\pi/4, 3\pi/4)$ . Dotted line : B-H, dashed line : interference term, solid line: TCS. (Right) Ratio of the interference to BH differential cross section  $\frac{d\sigma}{dy dt d\phi dQ^2}$  calculated for  $Q^2 = 4 \text{ GeV}^2$ ,  $t = -0.35 \text{ GeV}^2$  and  $\phi = 0$  for the GK (dashed) and G-MSTW (solid) models at NLO. From (a) to (c)  $p\text{Pb}$ ,  $\text{PbH}$  and  $p\text{H}$  cases.

## 5 Exclusive lepton-pair hadroproduction via odderon-pomeron fusion

Throughout this work, we have based our discussion on the idea that the (theoretical and experimental) requirements for selecting UPC collisions was *de facto* preventing hadronic interactions to take place or at least that photon-induced processes would be dominant. This is a rather safe assumption in nucleus-nucleus collisions where the coherent photon fluxes are enhanced by a factor  $Z^2$  for each nucleus, whereas double-pomeron-induced reactions only scale like  $A^{1/3}$ . It also seems a reasonable assumption for  $pA$  collisions that electromagnetic interactions dominate.

In the case of  $pp$  collisions, the  $Z^2$  factor is absent and the UPC requirements are also very similar, if not identical, in practice, to that for an exclusive or diffractive process. For instance, in order to impose  $b > 1/R_p$ , one can impose that the proton expected to emit the photon is only deflected by a  $\Delta p_t$  of say maximum 100 MeV, which corresponds to  $b \gtrsim 2$  fm. Such a requirement however may not be sufficient to prevent any scattering by the exchange of a pomeron or an odderon. In fact, the photon-pomeron process depicted on Fig. 4c should in principle be encompassed in the GPD description at high energies.

The production of a lepton pair in UPC which we discussed so far should thus be confronted to a potentially competing process leading to the same final state, in which the virtual photon decaying into lepton pair is produced in an Odderon-Pomeron (OP) fusion as depicted in Fig. 4d. This is similar to the situation occurring in the case of the central exclusive hadroproduction of a  $J/\psi$  studied in [33]. In this case, the  $J/\psi$  can be produced either by the photon-Pomeron fusion – that is the one expected for UPC – or by the OP fusion. In fact, the cross sections for both processes are similar at the Tevatron. Owing to the increase of the gap survival probability for lower energies, it is reasonable to believe that, at AFTER@LHC energies, *i.e.* around  $\sqrt{s_{NN}} = 115$  GeV, exclusive  $J/\psi$  production in  $pp$  collisions would be dominated by OP fusion.

Both production mechanisms are however characterized by a different  $J/\psi$  transverse-momentum dependence [33]. In particular, if one imposes that the final state protons have  $|t| > 0.25$  GeV<sup>2</sup>, the OP contribution can be enhanced ten times with respect to the photon induced one.

In the case of lepton-pair production in the conditions of UPC, a similar situation will likely occur. The experimental study of such a process with specific cuts on  $t$  may thus provide an unexpected path to the Odderon discovery via interference with the pure QED BH process in the same way as the TCS signal would be extracted in the region where it dominates. Despite its interest, the evaluation of the corresponding cross section along the line of [33] is far beyond the scope of the present work.

Similarly, the odderon could also contribute to the  $\eta_c$  production as recently discussed in [31].  $\eta_c$  can be produced by photon-odderon fusion due its different quantum number with respect to the  $J/\psi$ . In the  $pp$  case, the cross section we obtained from  $\gamma\gamma$  fusion is slightly larger than from photon-odderon fusion obtained in [31], both on the order of a picobarn or less. In the  $pPb$  and  $Pbp$  cases, the photon can be radiated by the ion and the pomeron by the proton. As we noted, although  $m_{\eta_c}$  is in principle above the so-called energy “cut-off”, the photon fluxes, even accounting from the minimum impact parameter

for a proton-lead UPC, is not zero. In the  $Pb p$  case, the photon-odderon induced cross section ranges from 30 up to 360 pb whereas the  $\gamma\gamma$  induced one is on the order of 440 pb. As for the dilepton case, a study of the transverse-momentum dependence should be able to discriminate between both processes.

## 6 Conclusion

We have theoretically investigated the feasibility of accessing the lepton-pair production in ultraperipheral collisions at the proposed fixed-target experiment AFTER@LHC, which takes advantages of the multi-TeV proton and ion beams of the LHC. To this aim, we have first estimated the magnitude of the cross section for lepton-pair production from the fusion of two quasi-real photons emitted by the quasi-grazing hadrons. This purely electromagnetic BH process can serve as an important tool for the determination of the luminosities with nucleon or ion beams but it can also be used for an experimental verification of the validity of the effective-photon approximation usually applied to estimate the flux of quasi-real photons emitted by these relativistically moving charges. Lepton-pair production also gives access to the proton GPDs via the TCS process. Another way to probe the photon flux is to measure  $\eta_c$  production for which the production rate in  $pp$  collisions at AFTER@LHC does depend on the minimal impact parameter used for the UPC.

The predictions which we obtained for the cross section for BH – using specific cuts relevant for the GPD extraction – are on the order of few thousand of pb for the  $pPb$  and  $Pb p$  cases and a slightly less than 10 pb for the  $pp$  case and we confirm the dominance of BH over TCS. This dominance can partially be overcome by studying of the interference – also sensitive on the GPDs – between TCS and BH which we evaluated at NLO. With specific cuts on the lepton polar angle, the ratio of this interference over the BH amplitude squared is on order of 10% with two models of GPDs, *i.e.* GK and G-MSTW. These are quite promising values giving hope for the extraction of this interference by means of the analysis of the azimuthal distribution of the produced leptons. Studying TCS in ultraperipheral collisions at a fixed-target experiment can also give us opportunity to study target polarization asymmetries, which are an useful tool to extract further information on GPDs [34].

We have also derived cross sections for  $\eta_c$  production by photon-pair fusion, which happens, in particular in this energy range, to be sensitive on the method used to compute the photon flux in the  $pp$  case. We found out that  $10^4$   $\eta_c$  can be produced per year in UPCs with AFTER@LHC.

Finally, we discussed possible competing hadronic processes via pomeron or odderon exchanges which could interestingly be separated out by a careful analysis of the transverse-momentum dependence of the produced particles.

In conclusion, AFTER@LHC offers a realistic possibility to study lepton-pair production in ultraperipheral collisions which opens the path to investigate features of the partonic structure of hadrons which are complementary to those studied with lepton beams. The

use of hadron beams may, for instance, offer the opportunity study to odderon-sensitive reactions.

## Acknowledgements

We thank D. d’Enterria, V.P. Gonçalves, S. Klein, R. Mikkelsen, J. Nystrand for useful discussions. This work is partly supported by the COPIN-IN2P3 Agreement, the Polish Grant NCN No DEC-2011/01/D/ST2/02069, and the CNRS grants PICS-06149 Torino-IPNO & PEPS4AFTER2.

## References

- [1] C. Adler *et al.* [STAR Collaboration], Phys. Rev. Lett. **89** (2002) 272302 [nucl-ex/0206004].
- [2] J. Adams *et al.* [STAR Collaboration], Phys. Rev. C **70** (2004) 031902 [nucl-ex/0404012].
- [3] S. Afanasiev *et al.* [PHENIX Collaboration], Phys. Lett. B **679** (2009) 321 [arXiv:0903.2041 [nucl-ex]].
- [4] B. Abelev *et al.* [ALICE Collaboration], Phys. Lett. B **718** (2013) 1273 [arXiv:1209.3715 [nucl-ex]].
- [5] E. Abbas *et al.* [ALICE Collaboration], Eur. Phys. J. C **73** (2013) 11, 2617 [arXiv:1305.1467 [nucl-ex]].
- [6] S. J. Brodsky, F. Fleuret, C. Hadjidakis and J. P. Lansberg, Phys. Rept. **522** (2013) 239 [arXiv:1202.6585 [hep-ph]].
- [7] H. Bethe and W. Heitler, Proc. Roy. Soc. Lond. A **146** (1934) 83.
- [8] E. R. Berger, M. Diehl and B. Pire, Eur. Phys. J. C **23** (2002) 675 [hep-ph/0110062].
- [9] B. Pire, L. Szymanowski and J. Wagner, Phys. Rev. D **83** (2011) 034009 [arXiv:1101.0555 [hep-ph]].
- [10] H. Moutarde, B. Pire, F. Sabatie, L. Szymanowski and J. Wagner, Phys. Rev. D **87** (2013) 5, 054029 [arXiv:1301.3819 [hep-ph]].
- [11] D. Müller, D. Robaschik, B. Geyer, F.-M. Dittes and J. Hořejši, Fortsch. Phys. **42** (1994) 101 [hep-ph/9812448].
- [12] X. D. Ji, Phys. Rev. Lett. **78** (1997) 610 [hep-ph/9603249].
- [13] A. V. Radyushkin, Phys. Rev. D **56** (1997) 5524 [hep-ph/9704207].
- [14] J. C. Collins and A. Freund, Phys. Rev. D **59** (1999) 074009 [hep-ph/9801262].
- [15] M. Diehl, Phys. Rept. **388** (2003) 41 [hep-ph/0307382].
- [16] A. V. Belitsky and A. V. Radyushkin, Phys. Rept. **418** (2005) 1 [hep-ph/0504030].
- [17] S. Boffi and B. Pasquini, Riv. Nuovo Cim. **30** (2007) 387 [arXiv:0711.2625 [hep-ph]].
- [18] M. Guidal, H. Moutarde and M. Vanderhaeghen, Rept. Prog. Phys. **76** (2013) 066202 [arXiv:1303.6600 [hep-ph]].
- [19] V. M. Budnev, I. F. Ginzburg, G. V. Meledin and V. G. Serbo, Phys. Rept. **15** (1975) 181.

- [20] A. J. Baltz, G. Baur, D. d’Enterria, L. Frankfurt, F. Gelis, V. Guzey, K. Hencken and Y. Kharlov *et al.*, Phys. Rept. **458** (2008) 1 [arXiv:0706.3356 [nucl-ex]].
- [21] J. P. Lansberg, V. Chambert, J. P. Didelez, B. Genolini, C. Hadjidakis, P. Rosier, R. Arnaldi and E. Scapparini *et al.*, PoS QNP **2012** (2012) 049 [arXiv:1207.3507 [hep-ex]].
- [22] A. Rakotozafindrabe, M. Anselmino, R. Arnaldi, S. J. Brodsky, V. Chambert, J. P. Didelez, E. G. Ferreira and F. Fleuret *et al.*, Phys. Part. Nucl. **45** (2014) 336 [arXiv:1301.5739 [hep-ex]].
- [23] L. Massacrier, M. Anselmino, R. Arnaldi, S. J. Brodsky, V. Chambert, W. d. Dunnen, J. P. Didelez and B. Genolini *et al.*, arXiv:1502.00984 [nucl-ex].
- [24] R. E. Mikkelsen, A. H. Sørensen and U. I. Uggerhøj, arXiv:1503.06621 [nucl-ex].
- [25] M. Drees and D. Zeppenfeld, Phys. Rev. D **39** (1989) 2536.
- [26] M. Drees, R. M. Godbole, M. Nowakowski and S. D. Rindani, Phys. Rev. D **50** (1994) 2335 [hep-ph/9403368].
- [27] G. Baur, K. Hencken, D. Trautmann, S. Sadovsky and Y. Kharlov, Phys. Rept. **364** (2002) 359 [hep-ph/0112211].
- [28] G. Racah, Nuovo Cim. **14** (1937) 93.
- [29] A. J. Baltz, Y. Gorbunov, S. R. Klein and J. Nystrand, Phys. Rev. C **80** (2009) 044902 [arXiv:0907.1214 [nucl-ex]].
- [30] K. A. Olive *et al.* [Particle Data Group Collaboration], Chin. Phys. C **38** (2014) 090001.
- [31] V. P. Goncalves and W. K. Sauter, arXiv:1503.05112 [hep-ph].
- [32] D. Mueller, B. Pire, L. Szymanowski and J. Wagner, Phys. Rev. D **86** (2012) 031502 [arXiv:1203.4392 [hep-ph]].
- [33] A. Bzdak, L. Motyka, L. Szymanowski and J.-R. Cudell, Phys. Rev. D **75** (2007) 094023 [hep-ph/0702134].
- [34] M. Boër, M. Guidal and M. Vanderhaeghen, arXiv:1501.00270 [hep-ph].

## A Kinematics

We denote the momenta of incoming nucleons (in the nucleon-nucleon cms) as:

$$\begin{aligned}
 p_A &= \frac{\sqrt{s}}{2} (1, 0, 0, \alpha), \\
 p_B &= \frac{\sqrt{s}}{2} (1, 0, 0, -\alpha),
 \end{aligned}
 \tag{A.1}$$

where the  $A$  is a nucleon from the beam,  $B$  is a nucleon from target and  $\alpha = \sqrt{1 - \frac{4M^2}{s}}$ . The Weizsäcker - Williams photon is emitted from a beam ( $\epsilon = -1$ ) or a target nucleon ( $\epsilon = +1$ ), and its momentum is given by:

$$k = x_\gamma \frac{\sqrt{s}}{2} (1, 0, 0, -\epsilon).
 \tag{A.2}$$

Momentum of outgoing lepton pair (or outgoing virtual photon decaying into heavy lepton pair) reads:

$$q = (q_0, q_T, q_z) \equiv (m_T \cosh y^{\ell\ell}, q_T, m_T \sinh y^{\ell\ell}), \quad (\text{A.3})$$

where  $m_T = \sqrt{q_T^2 + Q^2}$  and  $y^{\ell\ell}$  is the lepton-pair rapidity which can be expressed as

$$y^{\ell\ell} = \frac{1}{2} \epsilon \log \left( \frac{(Q^2 - t)(\alpha + 1)}{Q^2(\alpha - 1) - t(\alpha - 1 - 2x_\gamma) + sx_\gamma^2(\alpha + 1)} \right), \quad (\text{A.4})$$

where:

$$t \equiv (k - q)^2 = Q^2 - m_T \sqrt{s} x_\gamma e^{\epsilon y^{\ell\ell}}. \quad (\text{A.5})$$

Inverting Eq. (A.4), we can express  $x_\gamma$  as a function of  $y^{\ell\ell}$ :

$$x_\gamma(y^{\ell\ell}, t, Q, \epsilon) = \frac{-2t + \sqrt{4t^2 - 4s(Q^2 - t)(\alpha + 1)[(\alpha - 1) - (\alpha + 1)e^{-2\epsilon y^{\ell\ell}}]}}{2s(\alpha + 1)}. \quad (\text{A.6})$$

or combining Eq. (A.5) with Eq. (A.7) we easily get:

$$t = t(y^{\ell\ell}, q_T^2, Q, \epsilon), \quad (\text{A.7})$$

$$x_\gamma = x_\gamma(y^{\ell\ell}, q_T^2, Q, \epsilon), \quad (\text{A.8})$$

$$J = \frac{dt}{dq_T^2}. \quad (\text{A.9})$$

## B Compton form factors and generalised parton distributions

In this appendix, we give the expressions of the LO hard-scattering kernel  $T_i$  appearing in the expression of the Compton form factor  $\mathcal{H}$ ,  $\tilde{\mathcal{H}}$  and  $\tilde{\mathcal{E}}$ . At Born order, the hard-scattering kernel associated to the quark GPDs are given by

$$\begin{aligned} T_H^q(x, \eta) &= e_q^2 \left( \frac{1}{-\eta - x - i\epsilon} - \frac{1}{-\eta + x - i\epsilon} \right), \\ T_{\tilde{H}}^q(x, \eta) &= e_q^2 \left( \frac{1}{-\eta - x - i\epsilon} + \frac{1}{-\eta + x - i\epsilon} \right), \\ T_E^q(x, \eta) &= e_q^2 \left( \frac{1}{-\eta - x - i\epsilon} - \frac{1}{-\eta + x - i\epsilon} \right), \end{aligned} \quad (\text{B.1})$$

and those associated to the gluon GPDs are zero. The NLO hard-scattering kernels can be found in [9, 32].